Journal of Catalysis 259 (2008) 75–84

Contents lists available at ScienceDirect

Journal of Catalysis

www.elsevier.com/locate/jcat

Carbon tolerant Ni–Au SOFC electrodes operating under internal steam reforming conditions

Ilias Gavrielatos [a,b], Vasilis Drakopoulos [b], Stylianos G. Neophytides [b,*]

[a] Department of Chemical Engineering, University of Patras, Patras, Greece
[b] Foundation for Research and Technology, Institute of Chemical Engineering and High Temperature Chemical Processes (FORTH/ICE-HT), Stadiou str. Platani, GR26504, Rion Patras, Greece

ARTICLE INFO

Article history:
Received 9 February 2008
Revised 23 July 2008
Accepted 25 July 2008
Available online 3 September 2008

Keywords:
SOFC
Carbon deposition
Ni/YSZ
Au impregnation
NiAu/YSZ
CH_4 steam reforming
CH_4 partial oxidation

ABSTRACT

Carbon tolerant Ni/YSZ anode modified with 1% (atomic ratio) Au with respect to Ni was tested under methane rich steam reforming conditions. The electrode was proved to be highly tolerant to C deposits, even at methane to water ratios as high as 3, at temperatures ranging between 973–1173 K. The NiAu anode was prepared by in situ combustion synthesis at 873 K and sintered in air at 1123 K. The SEM images have shown that the Au modified Ni/YSZ electrode was nanostructured with particle size ranging between 50–100 nm.

1. Introduction

Fuel cells can be potentially one of the most important energy conversion tools of the 21st century. Fuel cell technology shows advantages concerning fuel efficiency, emissions, maintenance and noise pollution. For stationary applications, i.e. power plants or combined heat and power generation [1,2] the solid oxide fuel cell (SOFC) is generally one of the most promising technologies. One of the key aspects for the efficient operation of solid oxide fuel cells is the suitable choice of fuel. The most frequently used fuel is hydrogen, which is mainly produced by steam reforming of methane on Ni-based catalysts at temperatures ranging from 973–1173 K. However, solid oxide fuel cells can run directly on natural gas or other hydrocarbon fuels [3–13] without the need of an external reformer, thus improving and simplifying system integration. This is due to the catalytic action of the fuel exposed state of the art Ni–YSZ cermet anode surface for steam reforming of methane in the temperature range of SOFC operation.

According to this process, which is known in the literature as internal steam reforming of methane (ISRM), the Ni surface of the Ni–YSZ cermet anode catalyzes the steam reforming reaction of methane (reaction (1)) as well as the water–gas shift reaction (reaction (2)):

$$CH_4 + H_2O \rightarrow CO + 3H_2, \quad (1)$$

$$CO + H_2O \rightarrow CO_2 + H_2, \quad (2)$$

thus producing H_2, CO, and CO_2. The produced hydrogen and carbon monoxide can be readily oxidized electrochemically at the three phase boundaries (Ni/YSZ/gas), generating electricity:

$$H_2 + O^{2-} \rightarrow H_2O + 2e^-, \quad (3)$$

$$CO + O^{2-} \rightarrow CO_2 + 2e^-. \quad (4)$$

Although the presence of water at high H_2O/CH_4 ratio can inhibit or at least minimize the problem of carbon formation, however the Nernst potential decreases significantly thus resulting in lower cell efficiency. As it is also shown in this study experimentally, by feeding the anode with varying H_2O/CH_4 ratios the open circuit potential can decrease even up to 300 mV as compared to its value without the presence of steam. This can be understood according to the Nernst equation (5)

$$E_{OCP} = E^o - \frac{RT}{2F} \ln\left(\frac{P_{H_2O}}{P_{H_2} P_{O_2}^{1/2}}\right), \quad (5)$$

where E and E^o are the open circuit cell potential and standard potential respectively at a given temperature T. As it is shown E depends on the partial pressures (P_{H_2O}, P_{H_2}, P_{O_2}) of the reactants and products according to reaction (6):

$$H_2 + \frac{1}{2}O_2 \rightarrow H_2O. \quad (6)$$

* Corresponding author.
E-mail address: neoph@iceht.forth.gr (S.G. Neophytides).

0021-9517/$ – see front matter
doi:10.1016/j.jcat.2008.07.011

It is considered that CH_4 molecule does not participate in the electrochemical process. For example by assuming a typical CH_4/H_2O mixture 30 kPa/60 kPa at the inlet of the SOFC the open circuit potential can vary significantly along the reactor depending on the partial pressure of the produced H_2 along the reactor. The open circuit potential (OCP) at 1100 K at the reactor's outlet considering total conversion of CH_4, in the case of the aforementioned CH_4/H_2O reacting mixture (H_2 and H_2O partial pressures being 75 and 25 kPa respectively), is 983 mV, while for a non-humidified H_2 feed ($P_{H_2O} < 1 \times 10^{-3}$ kPa) the OCP can be as high as 1268 mV. The standard OCP at 1100 K is 969 mV. In addition high water content can cause the oxidation of Ni either affecting its electronic conductivity or inducing the delamination of the Ni/YSZ anode. Many studies in the literature have been devoted on carbon formation and deactivation of supported Ni steam reforming catalysts [7,13–26]. Carbon can be formed through the thermal cracking of CH_4/hydrocarbons (reaction (5)) or by the decomposition of CO (reaction (6)):

$$CH_4 \rightarrow C_{gr} + 2H_2, \tag{6}$$

$$2CO \rightarrow C_{gr} + CO_2. \tag{7}$$

There are many factors that influence the likelihood of carbon formation. The nature of the catalyst is very important as well, for example carbon deposition is more likely over nickel than ruthenium [27–29], or copper [30,31], or LSCM (and other complex perovskites) [32–35] catalysts. It has been suggested that Ru and Rh do not facilitate the formation of carbon deposits due to poor carbon solubility in these metals [36,37]. On the downside, Ru and Rh are prohibitively expensive. It has also been shown that small amounts of sulfur can suppress carbon poisoning by blocking carbon nucleation sites [38,39]. Gorte et al. [31] studied a Cu–YSZ anode, which proved quite stable for the oxidation of hydrocarbons. In addition, it has also been shown that Cu supported on ceria is a stable electrooxidation catalyst for the internal reforming of hydrocarbons [40–42]. Park et al. [30] obtained similar results while feeding *n*-butane and methane to YSZ/CeO_2/Cu anode for direct oxidation. In a more recent study, Sn/Ni surface alloy has been identified as much more carbon tolerant than monometallic Ni in the steam reforming of methane, propane and isooctane at moderate steam to carbon ratios [43]. Among the materials with perovskite structure, chromites and titanates are promising SOFC anodes [44–46]. Interesting results have been obtained with lanthanum strontium titanates [47] and especially cerium doped lanthanum strontium titanate [48]. LSCM also shows a stable electrode performance in methane [32].

The modification of catalytic activity against the formation of carbon deposits can be achieved by the addition/doping of small quantities of another metal on the surface of Ni particles of the Ni/YSZ anode. In a theoretical study, Besenbacher et al. [18] concluded that the presence of small amount of gold in a supported nickel catalyst can induce a significant effect on the carbon formation process during the steam reforming of methane. Very small amount of gold present in the nickel catalyst may decrease significantly the amount of carbon deposits on the electrocatalyst. Rostrup-Nielsen et al. [19], using density functional theory (DFT) calculations, have also predicted that Au inhibits methane dissociation. Triantafyllopoulos and Neophytides [49] studied the nature of carbon species that are formed on the Ni(1 at% Au)/YSZ catalyst during the dissociative adsorption of methane and obtained very interesting results that confirm the previous statement.

In the present work, the electrocatalytic activity and carbon tolerance of the Ni(Au 1 at%)/YSZ electrocatalyst is examined, under CH_4 rich steam reforming conditions. The electrocatalyst was prepared by in situ combustion synthesis, which was proved to be a very powerful technique for the preparation of nanostructured electrodes.

2. Experimental

The Ni(Au 1 at%)/YSZ electrocatalyst was prepared by the "in situ combustion synthesis" method. The process of "in situ combustion synthesis" makes use of the highly exothermic redox chemical reactions between metals and non-metals, while the metathetical (exchange) reaction between reactive compounds or reactions involves redox compounds/mixtures. The starting materials were $ZrO(NO_3)_2{\cdot}6H_2O$, $Y(NO_3)_3{\cdot}6H_2O$, $Ni(NO_3)_2{\cdot}6H_2O$ and urea ($CO(NH_2)_2$) as the fuel (F). $HAuCl_4$ was added as the precursor in the combustion mixture for the preparation of the NiAu composites. Nitrates in the required stoichiometric proportions and urea ($O/F = 1$) were mixed (together) in an alumina crucible together with the appropriate amount of $HAuCl_4$. The mixture was heated up to 363 K on a hot plate to remove water. Then it was cooled down at room temperature and its viscosity was controlled by the addition of ethanol absolute. A small amount of the mixture was applied on a YSZ pellet surface with a brush and then heated in a furnace at 873 K. At this temperature the combustion takes place in less than a minute and a layer NiAu/YSZ is formed. This procedure was repeated several times until a homogeneous film with thickness around 30 μm was formed on the pellet. Finally, the pellet was calcined at 1123 K to consolidate the film.

The catalysts prepared by the combustion synthesis were NiAu/YSZ containing 1, 2 and 5% Au atomic ratio (at%) with respect to Ni atoms. The Ni loading with respect to the whole sample was in all cases 50 wt% Ni. The BET surface area of the samples was measured by QuantaChromeAutosorb-1 BET and chemisorption system and was found 3 m^2/g. XRD measurements were carried out by the use of Philips PW18 XRD instrument. The particle size calculation was based on X-ray line broadening of the diffraction peak according to Scherrer's equation and the microstructure and bulk composition of the sample was studied by the use of SEM-EDX imaging (LEO SUPRA 35VP). The surface composition was determined by XPS measurements, which were carried out in a UHV equipped with a hemispherical analyzer (SPECS LH-10) and a twin-anode X-ray gun.

The catalytic and electrocatalytic experiments of Figs. 3, 5 and 7 were carried out on a NiAu(1 at%)/YSZ electrode with a geometric surface area of ≈1 cm^2 and the deposited amount of NiAu(1 at%)/YSZ was ≈18.8 mg. The transient and electrokinetic experiments depicted in Figs. 6 and 8 were carried out on 11.5 mg NiAu(5 at%)/YSZ of surface area ∼1 cm^2. The cathode side of the tested fuel cell system consisted of a porous LSM/YSZ electrode prepared by the screen-printing method. The flat YSZ electrolyte (130 μm thick), that was sandwiched in between the anodic and cathodic electrodes served also as the support for the single fuel cell system. Current collection was achieved through the use of platinum mesh for both the anode and cathode compartments. Both Pt meshes were well pressed on the electrodes, using springs, to achieve the best current collection possible. The planar fuel cell system was attached on a YSZ tube and sealed airtight by using a glass sealing. The anodic electrode was exposed to hydrogen/water or methane/water mixtures while the cathodic electrode was fed with air. Kinetic experiments and electrochemical measurements were performed at different temperatures and different methane and hydrogen partial pressures. The inlet and outlet of the reactor is monitored by a quadrupole mass spectrometer (BALZERS OMNISTAR). In this way the kinetics of the steam reforming reaction were studied and the carbon deposition rate was determined by checking the carbon and H_2 mass balances according to Eq. (7)

$$r_{H_2} = 3r_{CO} + 4r_{CO_2}. \tag{7}$$

The electrochemical measurements were carried out by an AMEL potentiostat/galvanostat model 7060.

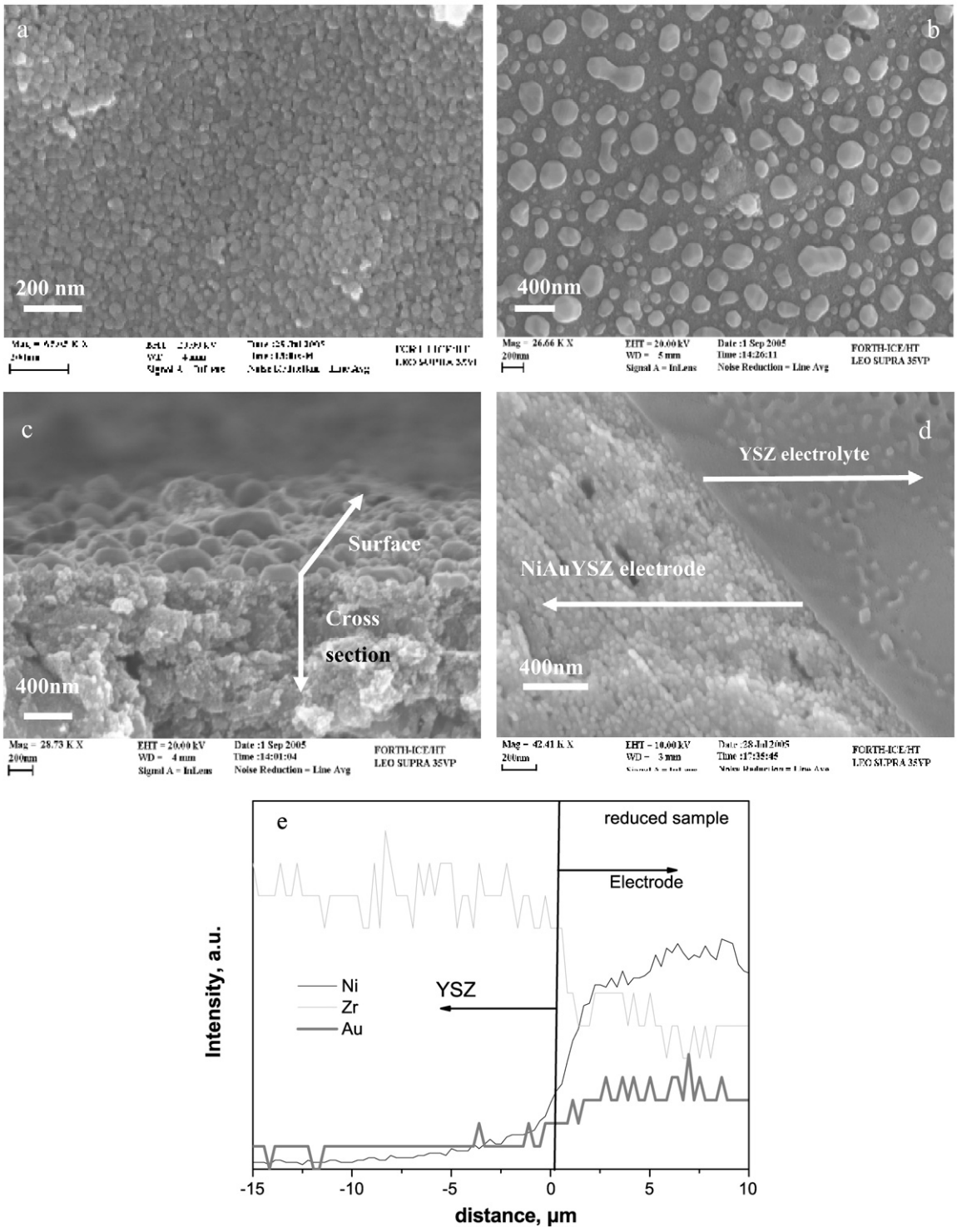

Fig. 1. Scanning electron micrographs of NiAu(1 at%)/YSZ electrode. (a) Top side before its reduction with H_2. (b) Top side after its reduction with H_2 for 2 h. (c) Cross section and surface/gas interface, (d) cross section and NiAuYSZ/YSZ interface, (e) SEM-EDX measurement of reduced NiAu(5 at%)/YSZ electrode scanning a cross surface area extending from the YSZ electrolyte into the bulk of the electrode.

3. Results

3.1. Physical characterization

The Ni(Au 1 at%)/YSZ electrocatalyst, prepared by the in situ combustion synthesis (described above), was characterized by scanning electron microscopy (SEM) and X-ray diffraction (XRD). Measurements were carried out before and after H_2 reduction. The SEM micrograph in Fig. 1a displays the surface of the Ni(Au 1 at%)/YSZ electrocatalyst in its oxidized state before the reduction process. The nanosize structure of the deposited film is due to the low temperature of the preparation method. The electrode is porous and consists of nanoparticles of the order of 30–40 nm. According to the XRD spectra depicted in Fig. 2 the film comprises discrete NiO or Ni and YSZ particles. This positive feature is expected to result in the increase of the active three phase bound-

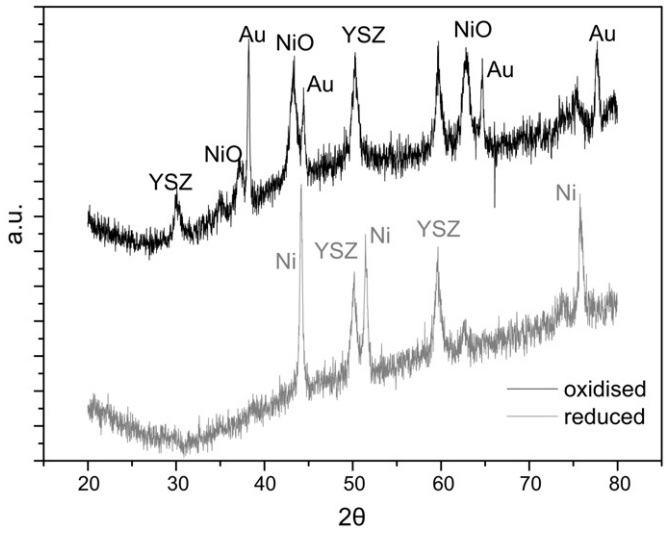

Fig. 2. X-ray diffraction spectrum of Ni(Au 5 at%)YSZ electrocatalyst before and after its reduction.

aries (t.p.b.) upon reduction between the gas phase, the catalytic particles and the YSZ solid electrolyte and consequently in the increase of electrocatalytic activity in total.

Before reduction the electrode is preheated at 1073 K under Air. Thereafter diluted hydrogen in argon (∼5% H_2/Ar) was fed at 1073 K for 2 h. The SEM image in Fig. 1b displays the surface of the electrode in its reduced state. In comparison to the previous SEM image (Fig. 1a), it is obvious that the reduction process has caused the formation of larger particles on the surface of the sample. The size of these larger particles is on the order of 100–200 nm and they only exist on the surface of the electrocatalyst. Further reduction did not result in the formation of larger particles. These larger particles were analyzed by the use of SEM-EDX and it has been found that they consist only of Ni. The space in between the large Ni particles is also composed of Ni and YSZ which certainly shows that Ni is not massively agglomerated in the larger Ni particles. Most probably due to its low content Au(1 at%) was not debatable by EDX analysis. It is worth noticing that the bulk of the electrocatalyst, which lies beneath these larger particles, seems to be unaffected by the reduction process. This is clearly shown in the SEM image of Fig. 1c, which displays a cross section area of the reduced Ni(Au 1 at%)/YSZ electrocatalyst. The image clearly shows that the large particles are observed only on the surface of the sample, while its bulk preserves its nanostructure. The agglomeration of Ni on the electrode's surface can be plausibly attributed to the lack of the YSZ nanoparticles, which in the bulk they most probably inhibit Ni sintering. The uniform distribution of Ni and Au throughout the bulk of the electrode is shown in Fig. 1e, which displays a SEM-EDX scan of the interface between the reduced NiAu(5 at%)/YSZ electrode and the compact solid YSZ electrolyte (presented in detail in Fig. 1d). As expected, the metallic Ni and Au concentrations rise from zero (inside the electrolyte) to a steady concentration level at the interface and inside the bulk of the electrode.

The XRD spectra of the NiAu(5 at%)/YSZ sample before and after reduction are depicted in Fig. 2. In the oxidized state (black line) the peaks that represent NiO and Au particles can be clearly seen. After reduction, very interestingly only Ni peaks are clearly detectable, while Au peaks have disappeared. Further investigation by means of XPS measurements proves the existence of gold on electrode's surface, thus suggesting that Au has been inserted into the lattice of Ni particles most probably at the surface. The Ni and YSZ particles' size based on Scherrer's equation is 28 and 16 nm respectively. This is in agreement with the particle size measured by the SEM images of Fig. 1. It is well known from literature that the incorporation of Au in Ni results in the formation of surface alloy [50,51]. In this respect, as it will be explicitly shown below, this affects the electrocatalytic and catalytic activity of electrode's surface operating under CH_4 steam reforming conditions.

3.2. Catalytic kinetic measurements

Kinetic experiments under internal steam reforming conditions were performed on the nanostructured NiAu(1 at%)–YSZ. The electrocatalyst was exposed to varying methane partial pressures (P_{CH_4}) up to 60 kPa at constant water partial pressure $P_{H_2O} =$ 5 kPa. The experiments were carried out within the temperature range of 973 to 1173 K. Fig. 3 clearly demonstrates the effect of P_{CH_4} on H_2 and CO formation rates at various temperatures and constant $P_{H_2O} = 5$ kPa. Reaction rates are positive order with respect to P_{CH_4} within the whole range of P_{CH_4} values. At higher temperatures reaction rate approaches maximum at P_{CH_4} values around 40 kPa. The positive reaction order and the appearance of a maximum at higher temperatures indicate that most probably the dissociative adsorption of methane can be the limiting step of the catalytic process in accordance to previous studies of CH_4 steam reforming reaction [20,49,52]. Nevertheless this is an argument that will be discussed further on. It is worth noticing that CO_2 formation rate was negligible. This shows that the presence of Au inhibits the catalytic rate of either water gas shift reaction (5) or CO disproportionation reaction (6). Though the experiments were carried out at CH_4/H_2O ratios exceeding by far unity, Ni(Au 1 at%)/YSZ electrocatalyst was shown to be very stable even at the elevated temperature of 1173 K and methane partial pressure as high as 50 kPa.

The mass balances of the system within the whole temperature range are presented in Fig. 3c. The theoretical mass balance equation based on the stoichiometry of reactions (1) and (2) is represented by Eq. (7). Fig. 3c shows that the experimental mass balances appear to be in good agreement with the theoretical equation (7) (straight solid line without symbols in Fig. 3c). Therefore, since the straight lines for all temperatures coincide it is rational to consider that no carbon deposition takes place on the NiAu/YSZ electrocatalyst. The slight deviation that appears in all four temperatures, can be attributed to error in the calibration of the mass spectrometer. Even when operating the reactor at higher temperatures, still no degradation of the catalyst was observed within the time scale of the kinetic experiments. The reproducibility of the catalytic performance was successfully verified (not shown here for brevity) on another sample under similar conditions and CH_4 partial pressures up to 20 kPa at constant $P_{H_2O} = 5$ kPa.

This very impressive performance for the Ni(Au 1 at%)/YSZ electrocatalyst is further supported by TGA experiments, performed on NiAu samples under dry CH_4 flow. Fig. 4a depicts isothermal thermo gravimetric experiments of NiAu(2%)/YSZ, NiAu(5%)/YSZ and the 'conventional' Ni/YSZ catalyst under dry 10% CH_4/Ar flow at $T = 923$ K. It is obvious that Ni/YSZ electrode shows immediate and rapid weight increase, due to carbon deposition on the Ni surface, whereas in the case of NiAu samples no weight increase was observed. This shows that Au modifies the catalytic activity, thus inhibiting methane's dissociative adsorption or at least the dehydrogenation reaction steps that lead to carbon formation. However carbon deposition on the NiAu sample is observed at higher temperatures as depicted by the temperature programmed gravimetric experiment of Fig. 4b. The turn over rate of the deposited carbon species is calculated by differentiating the plots in Fig. 4b with respect to time and is plotted against $1/T$ in Fig. 4c. As it is evident carbon deposition takes place on NiAu/YSZ sample at temperatures above 923 K. By comparing the slopes of the two samples in Fig. 4c it is easily concluded that the reaction on NiAu/YSZ is a highly ac-

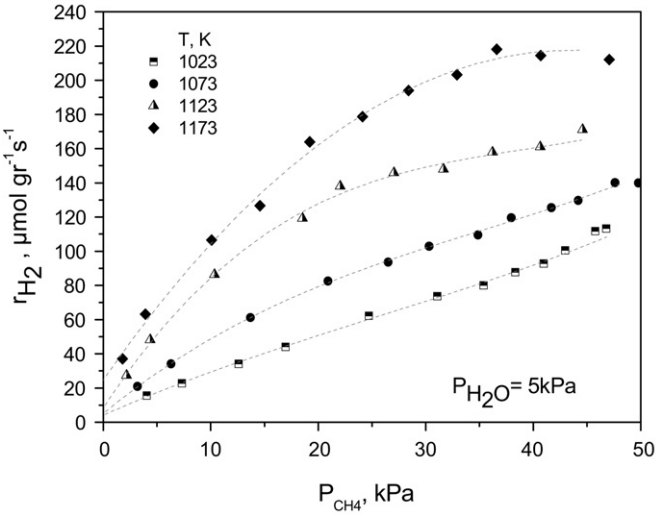

(a)

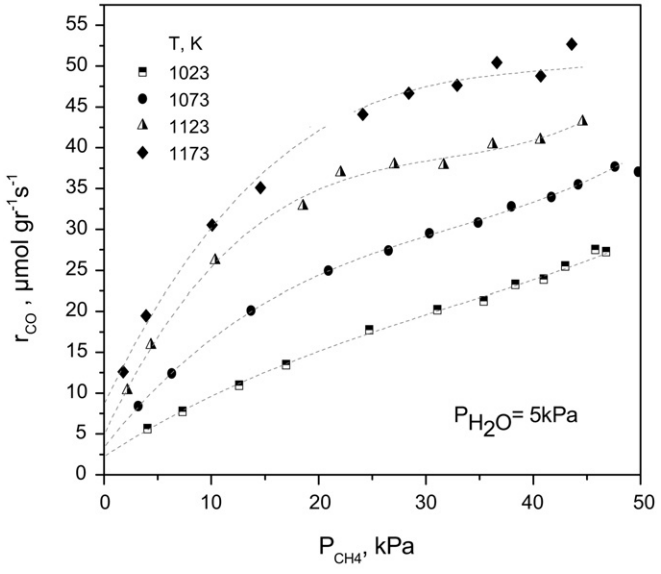

(b)

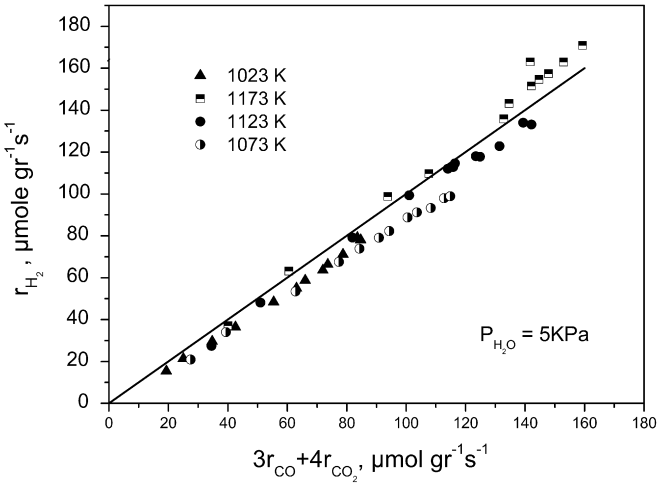

(c)

Fig. 3. Catalytic kinetic effect of P_{CH_4} on H_2 (a) and CO (b) formation rates. (c) Stoichiometric correlation of H_2 and carbon oxides formation rates at various temperatures and constant $P_{H_2O} = 5$ KPa (see Eq. (7)).

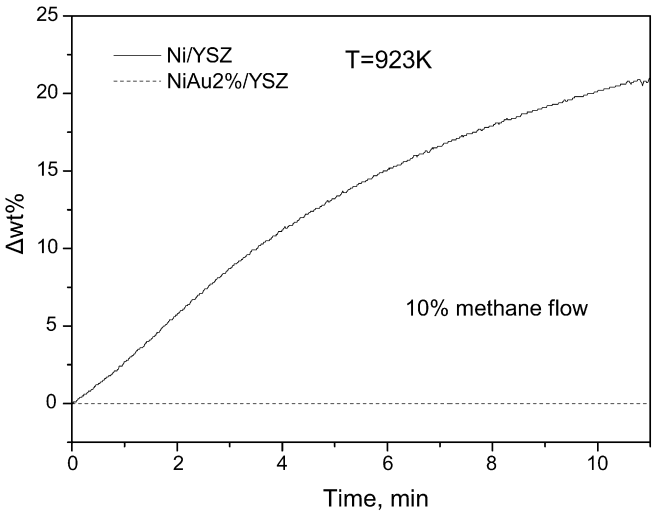

(a)

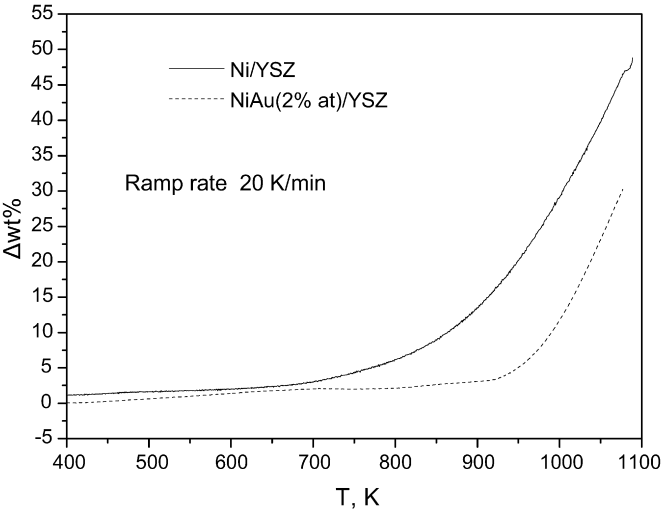

(b)

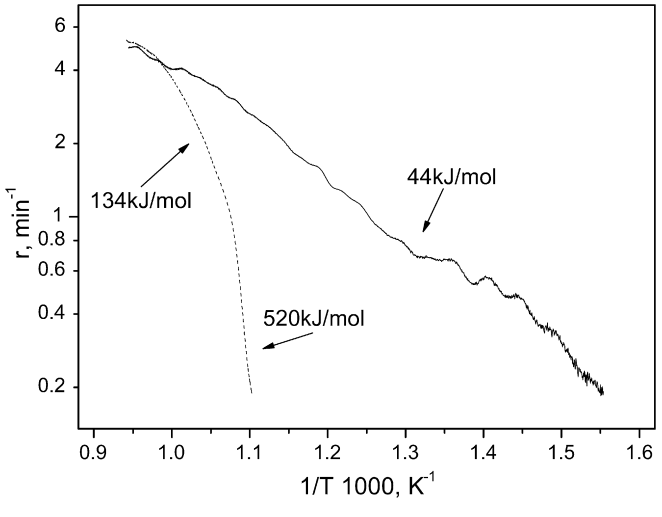

(c)

Fig. 4. Thermogravimetric experiment (TGA) of NiAu(1 at%)/YSZ and Ni/YSZ samples under 10% CH_4/Ar dry methane flow. (a) Isothermal $T = 923$ K, (b) linear temperature variation 20 K/min, (c) Arrhenius plots of the data depicted in Fig. 4b.

tivated process (520–134 kJ/mol), as compared to that on Ni/YSZ (44 kJ/mol), especially at the initial stages of carbon deposition.

3.3. Electrocatalytic behavior

The electrochemical behavior of the Ni(Au 1 at%)/YSZ anode was investigated by performing several electrochemical measurements under internal steam reforming conditions at different temperatures, ranging from 1023 to 1123 K and different methane/water ratios, ranging from 1 to 3. The total flow rate was 83–107 cc/min, while the methane flow was adjusted between 5–20 cc/min, depending on the methane partial pressure that was fed to the anode. Figs. 5a–5c depict the results with respect to O^{2-} electrochemical flux obtained at 1123 K and at methane to water ratios 1.01, 2.1 and 3.22 respectively. The steam reforming reaction produces H_2, CO and very small amount of CO_2 at open circuit conditions. Under fuel cell operating conditions, hydrogen and carbon monoxide are electrochemically oxidized producing water, carbon dioxide and electricity. CH_4 conversion was between 10–15%. It is interesting to notice that at lower CH_4/H_2O ratios limiting current is reached due to H_2 starvation, while in all cases the sum of the carbon oxides produced either remains constant (Fig. 5c) or slightly decreases (Figs. 5a and 5b) with increasing current. This strongly indicates that CH_4 does not participate directly in the electrochemical oxidation process. In this respect the variation in the open circuit potential can be attributed to the variation of the H_2/H_2O because of the increase of the catalytic rate of the steam reforming reaction upon increasing CH_4 partial pressure. Thus according to the Nerst equation (5) which takes into consideration only H_2 oxidation reaction the open circuit potential is estimated to vary from 891 mV (Fig. 5a $P_{H_2} = 2.7$ kPa) to 985 mV (Fig. 5c, $P_{H_2} = 8.7$ kPa). The experimental and estimated values are shown in Table 1. It is evident that the experimental and theoretically estimated values are rather close. The deviation can be attributed to the mixed potential induced by the presence of CO, which is an electroactive species and is not included in the used Nerst equation (5).

In order to shed more light on the reaction mechanism and the effect of Au doping on the electro catalytic activity of methane reforming/oxidation the transient experiments depicted in Fig. 6 were carried out. Initially dry methane/Ar mixture (total flow ~100 cc/min with ~4.5 kPa CH_4) is being processed over the NiAu(5 at%)/YSZ anode at 1023 K. The interaction of CH_4 with the Ni surface results as expected in the formation of H_2 and apparently to deposited carbon on the Ni surface. The open circuit voltage was $V_{OCP} = -1486$ mV. At time $t = 0$ a constant potential $V = -1200$ mV is applied corresponding to a current density $i \approx 4.3$ mA/cm^2. Surprisingly the formation rate of H_2 drops below 50% (Fig. 6a) accompanied by CO formation. No water or CO_2 formation was detected. Thereafter H_2 formation rate increases to a steady value corresponding to the stoichiometry of methane's partial oxidation according to reaction (8):

$$CH_4 + \frac{1}{2}O_2 \rightarrow CO + 2H_2. \quad (8)$$

It must be noted that CO formation rate slightly decreases and corresponds directly to the current variations. This apparently shows that only CO is produced by the electrochemical oxidation of the adsorbed carbonaceous species on the NiAu(5 at%)/YSZ anode. It is interesting to notice that similar experiment at lower temperatures (873 K Fig. 6b) shows the formation of CO_2 and H_2O most probably due to the direct oxidation of CO and H_2. As it will be shown further on, this can be attributed to the limited decomposition reaction rate of oxyhydrogenated adsorbed species through which the formation of CO and H_2 (reaction (12)) is carried out. The reaction rates of the products formation, during the transient

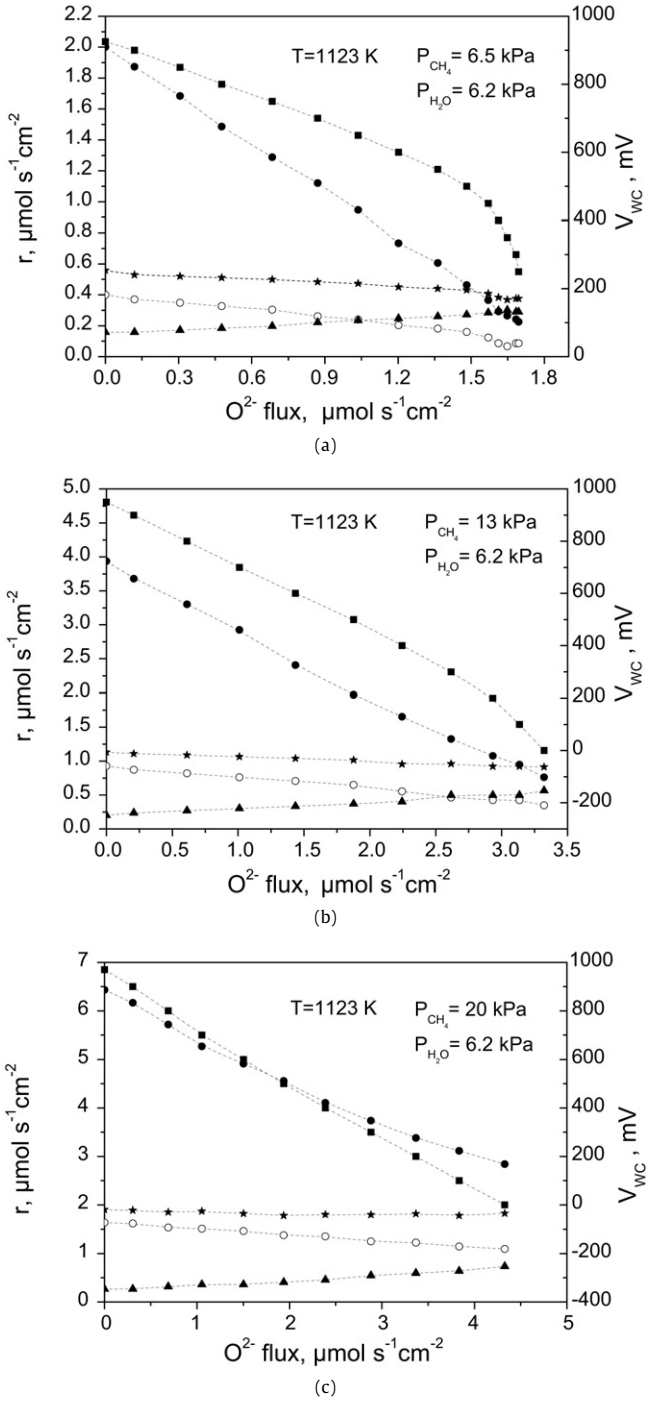

Fig. 5. Electrokinetic measurements under internal steam reforming conditions at $T = 1123$ K and CH_4/H_2O ratios: (a) 1.05 ($F_t = 83$ cc/min), (b) 2.1 ($F_t = 104$ cc/min), (c) 3.22 ($F_t = 107$ cc/min). (■, V_{WC}; ∗, r_{CH_4}; ●, r_{H_2}; ○, r_{CO}; ▲, r_{CO_2}.)

Table 1
The effect of CH_4 reforming rate on OCP at $P_{H_2O} = 6.2$ kPa, $T = 1123$ K (Fig. 5)

P_{CH_4}	r_{H_2} (μmol s^{-1} cm^{-2})	P_{H_2} (kPa)	E_{OCP} experimental (mV)	E_{OCP} theoretical (mV)
6.5	2.05	2.7	922	900
13	3.95	5.3	946	922
20	6.50	8.7	971	945

experiments of Fig. 6, are comparable to the applied current density. In particular as shown in Fig. 6 the applied current density 4.3 mA/cm^2 corresponds to 0.022 μmol O^{2-}/cm^2 s which is comparable to the 0.06 μmol H_2/cm^2 s that are being produced by CH_4

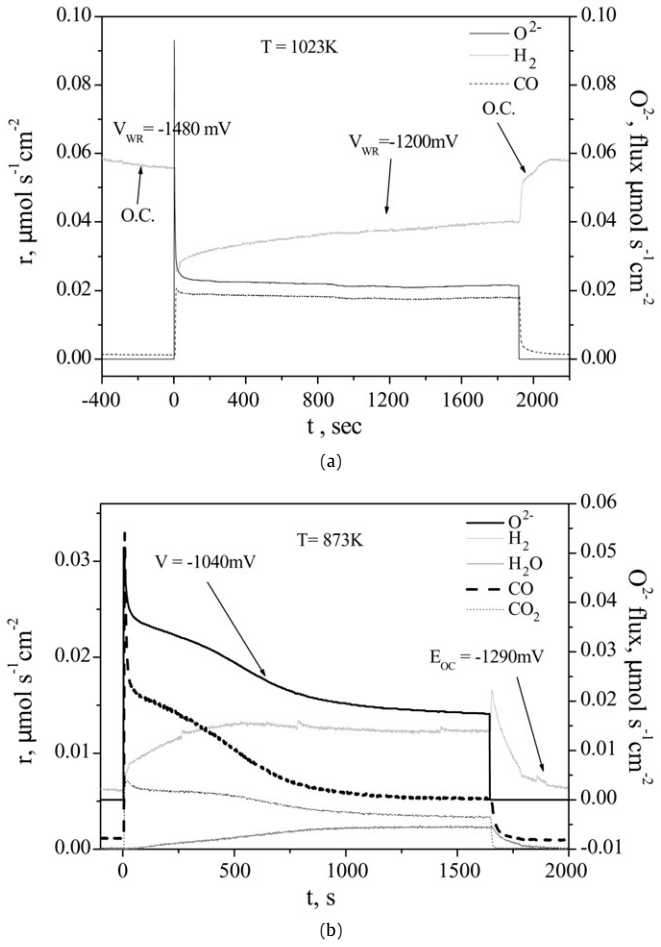

Fig. 6. Dynamic response of the production rate of H_2 and CO at $T = 1023$ K: (a) H_2, CO, CO_2 and H_2O at $T = 873$ K, (b) on NiAu(5 at%)/YSZ upon constant voltage application ($F_t = 100$ cc/min).

dissociation. Thus it is quite reasonable to observe the aforementioned effect on the open circuit reaction rate of CH_4 dissociation.

3.4. Stability test

The stability of the anode was tested through the short term durability test depicted in Fig. 7. The Ni(Au 1 at%)/YSZ anode was fed with ~22 kPa methane and ~6 kPa water. Pure oxygen was fed to the cathode and the cell operated at 1123 K and −500 mV (V_{cell}) producing about 300 mA/cm^2 for more than 60 h. The performance of the cell was stable throughout the experiment. The electrochemical performance of the cell under H_2 flow was tested, before and after the 60 h stability test, to check if any degradation took place. In order to simulate the gas composition produced by the reforming reaction the flow was composed of 10% hydrogen and 4.2% water in Ar and the cell was tested at $T = 1123$ K. As shown in Fig. 7 the cell performed exactly the same before and after the durability test, which further proves the high tolerance of the NiAu/YSZ electrocatalyst to carbon deposition, under internal steam reforming conditions.

4. Discussion

4.1. Physicochemical properties

The in situ combustion synthesis method for the electrode preparation is not a state of the art procedure. However by following this method it was possible to prepare the electrode at low

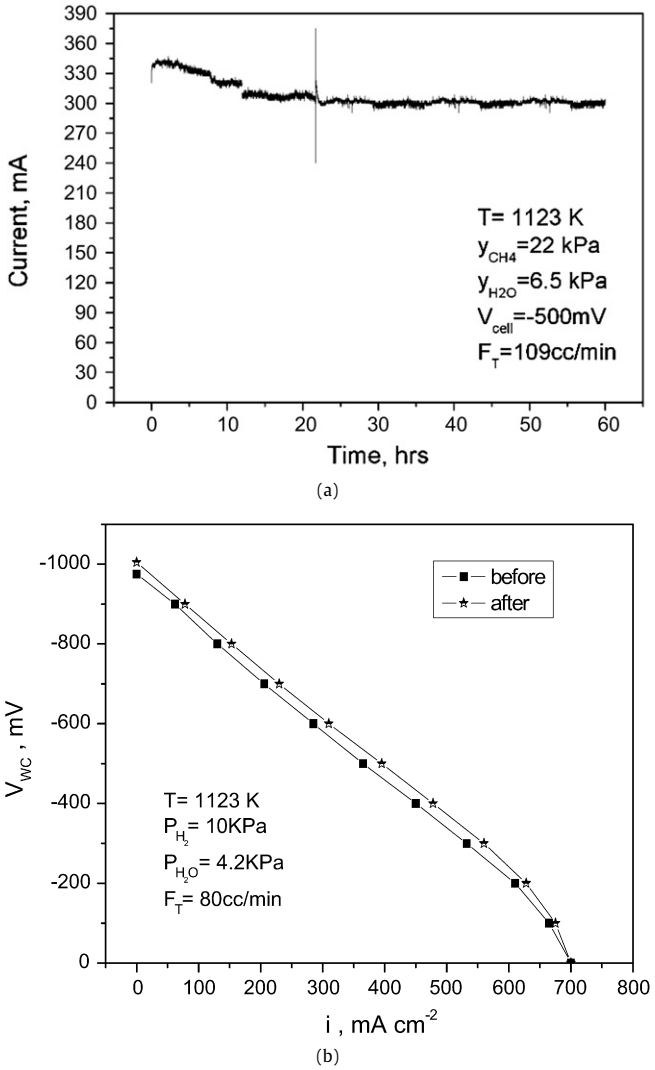

Fig. 7. (a) Short term stability test of the anode at $T = 1123$ K, $CH_4/H_2O > 3$ and operating voltage $V_{cell} = -500$ mV. (b) Electrocatalytic performance under 10% H_2 and 4.2% H_2O at $T = 1123$ K, before and after the stability test.

firing temperatures (<1073 K), so that the simultaneous processing of Au into the Ni/YSZ electrode structure was possible. In addition due to the low preparation temperature the electrode is composed of nanoparticles (Fig. 1) with size ranging between 30–50 nm. In contrast, by following the normal preparation procedures (firing temperatures 1673 K) particle sizes as large as 1–2 μm are formed. The nanostructure nature of the electrode is expected to result in:

- Larger catalytic surface area. The BET surface area of the combustion synthesis Ni/YSZ electrocatalyst is 3 m^2/gr and it is by a factor of 5 larger than the high temperature fired Ni/YSZ.
- Extended three phase boundaries between the electrocatalyst and solid electrolyte (Fig. 1d). Though the nanosized catalytic particles are beneficial for the high surface area of conventional catalytic systems in the present case the particle size of the Ni agglomerates play significant role in the bulk conductivity of the electrode. It must be mentioned that by reducing the samples at lower temperature (873 K) the electrode film had a non-acceptable low conductivity. However the nanoparticle structure of Ni must be further optimized by adjusting the sintering temperature in order to achieve higher electronic conductivity through the electrode layer, while maintaining extended interface.

- Higher resistivity towards thermal sintering of Ni particles. Though this statement has not yet been proved on a long term basis, nevertheless the intercalation of the YSZ nanoparticles is expected to obstruct the agglomeration of Ni nanoparticles. Within the short timeframe of the electrode treatment under H_2 as shown in Figs. 1b and 1c the agglomeration of the particles is rather obvious on the surface than in the bulk of the material.

As has been mentioned above, upon reduction of the sample Au is inserted into the lattice of the Ni particles. The estimated Au/Ni atomic ratio (=0.11), as derived by dividing the calibrated Au and Ni XPS peak areas, is twice as large than the nominal composition of the Au content with respect to Ni (5 at% Au). This strongly indicates that Au is mainly accumulated on the Ni surface in accordance to the literature, which reports that Au forms surface alloy on the Ni surface [53,54]. This behavior is also expected by the miscibility gap in the Ni–Au phase diagram [54]. Sinfelt since 1973 described [55,56] that, it is possible to create bi-metal clusters also when the two metals are not miscible. Chin et al. [51] showed by the use of EXAFS, that the Au–Ni bond exists on the Ni surface with lower coordination number (5.3) in contrast to the high coordination number (12) that was estimated for Au–Au bond in Au particles. Of course there's always the possibility that part of Au may diffuse in the bulk of Ni particles. For example, at temperatures higher than 923 K Holmblad et al. [54] observed diffusion of Au into the bulk and most probably a temperature dependent equilibrium is established between surface and bulk solid solutions. Besenbacher et al. [18] by using DFT calculations had shown that the Au atoms are inserted in the surface lattice of the Ni particles thus affecting the electronic/catalytic properties of the neighboring Ni atoms. In a more recent publication Bengaard et al. [57], who carried out more detailed DFT calculations, proposed that Au is located on the step edges of Ni on which it preferentially binds.

4.2. Kinetic and electrokinetic mechanism

The electrokinetic experiments of Fig. 5 show that methane is not oxidized electrochemically even when H_2 and CO are completely converted thus reaching limiting current (Fig. 5a). This strongly indicates that either H_2O adsorbed species or electrochemically supplied O^{2-} oxidize an intermediate adsorbed hydrogenated carbon species (CH_x) resulting from the sequential dehydrogenation of CH_4. The limiting step can be located either at a stage prior to the oxidation step along the dehydrogenation sequence or at a stage after the oxidation of the adsorbed CH_x species.

Triantafyllopoulos and Neophytides [49] proposed that the synthesis gas production proceeds through the decomposition of oxyhydrogenated carbon species, which are formed by the oxidation of CH_x species according to the following reaction scheme (reactions (8)–(11)):

$$CH_4 \rightarrow CH_x + \frac{4-x}{2}H_2, \tag{8}$$

$$CH_x \rightarrow C + \frac{x}{2}H_2, \tag{9}$$

$$CH_x + O_{ad} \rightarrow CH_xO, \tag{10}$$

$$C + 2O_{ad} \rightarrow CO_2. \tag{11}$$

The carbon species formed by reaction (9) are carbidic species [49,52], which readily react with adsorbed O_{ad} to produce CO_2 (reaction (11)). In addition at these elevated temperatures the reaction between CH_x fragments to form adsorbed C_2 and H_2 can also govern the stability of the catalysts as this can facilitate the graphite formation. The oxidation of CH_x species formed through reaction (8) is expected to result in the formation of oxyhydrogenated species CH_xO (reaction (10)). The adsorbed O_{ad} species can be generated either by the dissociative adsorption of H_2O or the electrochemical O^{2-} supply. Thermal decomposition of CH_xO species results in the formation of CO and H_2 according to reaction (12):

$$CH_xO \rightarrow CO + \frac{x}{2}H_2. \tag{12}$$

The relative magnitude of the rates of reaction steps (9) and (10) will determine the carbon tolerance of the steam reforming process. Thus a carbon tolerant catalyst must be able to catalyze the oxidation of the intermediate CH_x species faster than their catalytic dehydrogenation towards C species formation. This can be accomplished either by retarding the sequential dehydrogenation of methane (reaction (9)) or by promoting the oxidation of the CH_x species (reaction (10)). The validity of the aforementioned considerations is proved by the transient experiment depicted in Fig. 6 and has been described in the results. Initially the dehydrogenation reactions (8) and (9) take place producing H_2 and apparently carbon deposits. The fast decrease of H_2 formation rate upon constant potential application (at $t = 0$) must be related to the interruption of the sequential dehydrogenation due to the oxidation of hydrogenated carbon species according to Eq. (10). Thereafter the CO and H_2 formation rates originate from the decomposition of the oxyhydrogenated species according to reaction (12). The progressive increase of H_2 formation and the slight decrease of CO production rate must be related to the direct oxidation of the initially deposited C species at $t < 0$ according to reaction (13):

$$C + O_{ad} \rightarrow CO. \tag{13}$$

In this respect C is depleted from the catalytic surface thus releasing active sites so that the formation rate of H_2 progressively increases to its steady state value. In the case of CO formation a significant portion of the rate upon voltage application is attributed to the oxidation of the already deposited carbon (reaction (13)), while further on, its formation rate proceeds mainly through reaction (12). This is also corroborated by the fact that the rates of CO and H_2 are not balanced initially i.e. at $t = 0$ upon voltage application, so that $2r_{CO} = r_{H_2}$. In addition from the transient experiment of Fig. 6, it becomes clear that the limiting step is the decomposition of the oxyhydrogenated species (reaction (12)). This is deduced by the fact that the steady state reaction rate of H_2 formation is lower than the corresponding reaction rate of H_2 (at $t < 0$) originating from the decomposition of CH_4 according to reactions (8) and (9). Taking into consideration the transient experiment of Fig. 6b that was carried out at lower temperature (873 K) it can be concluded that the dissociative adsorption of methane is an equilibrium reaction step. This conclusion is derived by the fact that the open circuit decomposition rate of CH_4 towards the production of H_2 is lower than the rate of H_2 formation under current application. The fact that CO_2 and H_2O production is observed, in contrast to the transient experiment at higher temperature (Fig. 6a), strongly confirms the conclusion that the decomposition of the CH_xO species is rate limiting, due to the lower decomposition rate at the lower temperature. In this respect the excess O^{2-} supply will therefore result in higher O_{ad} coverage and consequently to the oxidation of CO and H_2. According to Ref. [58] under these lower T conditions (Fig. 6b), the temperature is not sufficient to push the adsorbed CO and H_2 from the surface before they are oxidized to CO_2 and H_2O respectively. In this respect it can be considered that at lower temperatures (873 K) the surface concentrations of adsorbed CO and H_2 are higher and the reaction between these adsorbates and the adsorbed O is allowed to take place and results in the formation of CO_2 and H_2O.

In accordance to the aforementioned considerations it is evident that the inhibition of C formation depends on the relative

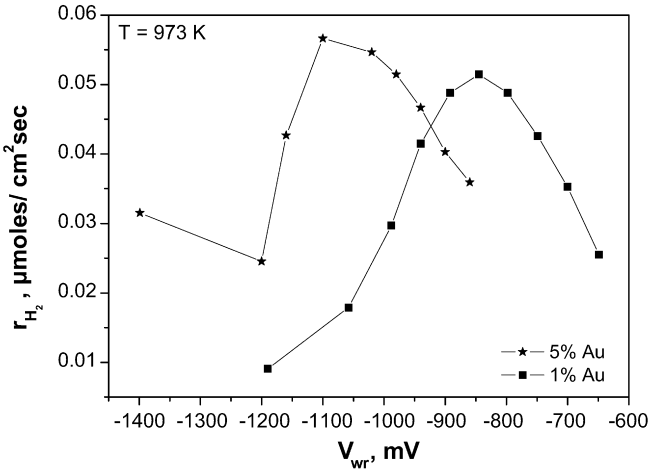

Fig. 8. H_2 formation rates versus anode's voltage with respect to an O_2 reference electrode (V_{WR}) for the NiAu(1 at%)/YSZ and NiAu(5 at%)/YSZ at $T = 973$ K.

reaction rates of the oxidation reaction (10) (r_{ox}) and the dehydrogenation reaction (9) (r_C). Thus a carbon resistant CH_4 steam reforming or oxidation catalyst must be considerably active towards the promotion of the r_{ox} than the r_C reaction so that $r_{ox} \gg r_C$. A strong indication that supports the promotional effect of Au content on r_{ox} is the electrokinetic experiment depicted in Fig. 8, where the H_2 formation rate is plotted with respect to the applied cell voltage. The decrease in the reaction rate after the maximum is due to the formation of H_2O and CO_2 at the expense of H_2 and CO. This corroborates with the aforementioned statement regarding the increase of the O_{ad} species coverage. In fact the decrease of the applied cell potential results in higher current application and thus higher O^{2-} flux is pumped to the NiAu/YSZ anode. This is equivalent to the increase of the O_2 partial pressure in the case of a conventional catalytic system. According to Langmuir–Hishelwood kinetic considerations the appearance of the maximum corresponds to a threshold where the coverage of the adsorbed hydrogenated species is lowered, while the increase in O_{ad} coverage is not adequate to maintain the increase of the adsorbed CH_x species oxidation rate (reaction (10)).

As it is evidently shown both H_2 formation rate maxima and open circuit potential are shifted towards more negative values. This shows that the electrocatalytically active species that are being formed by the dissociative adsorption of methane induce higher cell potential. Based on the Nernst equation (14) the higher absolute value of cell potential is caused by the decrease of O_{ad} activity a_0 on the NiAu/YSZ electrode [59].

$$E_{OC} = \frac{RT}{2F} \ln\left(\frac{a_0}{P_{O_2}}\right). \tag{14}$$

This is directly related to the depletion of O_{ad} from the electrode surface either due to the higher reactivity of the adsorbed carbonaceous species with O_{ad} or O^{2-} species or to the displacement of the O_{ad} species by the adsorbed carbonaceous species. The shift of the reaction maximum towards more negative potential for the case of NiAu(5%)/YSZ can be an indication of either a slower CH_4 dissociation rate or less reactive (stronger surface bonding) carbonaceous species towards CO production.

Besenbacher et al. carried out ab initio theoretical calculations [18] and predicted that the addition of small amount of Au on the Ni surface induces such changes on the catalytic/electronic properties of Ni surface, so that both the activation barrier of CH_4 dehydrogenation and the potential energy of the resulting carbon/carbonaceous species increase. The significant increase in activation energy is shown in the TGA experiments of Fig. 4c. Interestingly an almost constant slope is observed in the Arrhenius plot of Ni/YSZ (Fig. 4c) which gives an activation energy of 44 kJ/mol. A significant number of both experimental and theoretical studies has been devoted to the understanding of the dissociative chemisorption of methane on Ni surfaces [18,54,60–63]. Both thermal desorption and kinetic studies [59,60] and molecular beam experiments [54] have been used to probe the nature of "C–H bond activation" on Ni, as well as on other metal surfaces [62]. The activation barriers determined from thermal adsorption and molecular beam experiments range between 50 and 91 kJ/mol [54,59,60] while activation energies as high as 100 kJ/mol were estimated, based on theoretical model calculations [18,61]. The constant activation energy shows that the Ni/C layer develops stable catalytic properties already in the early stages of carbon deposition. This can be due to the graphitization of the Ni surface, which thereafter promotes constantly the autocatalytic graphite formation [64,65]. On the other hand in the case of NiAu/YSZ a tenfold larger activation energy is observed initially which upon the built up of carbon deposits it approaches, at elevated temperatures, the activation energy of Ni/YSZ sample. This can be realized if we assume that the Ni/C layer undergoes significant modifications resulting finally into a graphitic layer that promotes the autocatalytic graphite formation.

In general two parameters can be considered for the graphite development on Ni surface. On the one hand a critical ensemble of Ni surface atoms is needed for graphite formation [38], while a rather strong bonding of the C species with the Ni surface may not facilitate the carbon–carbon reaction. This is in qualitative agreement with the experimental observation in the TGA experiment of Fig. 4c, which shows that in the case of NiAu/YSZ sample a larger carbon deposit must be reached so that the activation energy of carbon deposition and obviously of graphite formation will match that of Ni/YSZ.

5. Conclusions

Despite its technical limitations, the in situ combustion synthesis method is an effective method for preparing porous, nanostructured electrocatalysts with high electrocatalytic activity. The Ni(1 at% Au)/YSZ electrocatalyst performs very well when operating with methane under internal steam reforming conditions, even when it is fed with high methane concentrations at temperatures as high as 1173 K. In this respect the Ni(1 at% Au)–YSZ electrocatalyst, prepared by combustion synthesis, proved to be a promising SOFC anode, because of its high tolerance to carbon deposition, at least under internal steam reforming conditions.

Acknowledgments

This work has been carried out within the framework of the Real_SOFC IP project Contract 502612, with the financial support of the European Commission.

References

[1] R.A. George, J. Power Sources 86 (2000) 134–139.
[2] John T.S. Irvine, J. Power Sources 136 (2004) 203–207.
[3] A.L. Lee, R.F. Zabransky, W.J. Huber, Ind. Eng. Chem. Res. 29 (1990) 766.
[4] S. Bebelis, S. Neophytides, C.G. Vayenas, in: U. Bossel (Ed.), Proceedings of the 1st European SOFC Forum, Lucerne, Switzerland, vol. 1, 1994, pp. 197–206.
[5] I.V. Yentekakis, Y. Jiang, S. Neophytides, S. Bebelis, C.G. Vayenas, Ionics 1 (1995) 491.
[6] M. Stoukides, Catal. Rev. Sci. Eng. 42 (2000) 1.
[7] A. Abudula, M. Ihara, H. Komiyama, K. Yamada, Solid State Ionics 86–88 (1996) 1203.
[8] T. Horita, N. Sakai, T. Kawada, H. Yokokawa, M. Dokiya, J. Electrochem. Soc. 143 (1996) 1161.
[9] V.V. Gal'vita, V.D. Belyaev, A.K. Demin, V.A. Sobyanin, Appl. Catal. A 165 (1997) 301.

[10] X. Zhang, S. Ohara, H. Chen, T. Fukui, Fuel 81 (2002) 989.
[11] C. Lu, W.L. Worrell, C. Wang, S. Park, H. Kim, J.M. Vohs, R.J. Gorte, Solid State Ionics 152-153 (2002) 393–397.
[12] J.B. Wang, J.-C. Jang, T.-J. Huang, J. Power Sources 122 (2003) 122.
[13] J. Liu, S.A. Barnett, Solid State Ionics 158 (2003) 11.
[14] J.R. Rostrup-Nielsen, in: J.R. Anderson, M. Boudart (Eds.), Catalytic Steam Reforming, Catalysis, Science and Engineering, vol. 5, Springer-Verlag, Berlin, 1984.
[15] M.V. Twigg, Catalyst Handbook, second ed., Wolfe Publishing, London, 1989.
[16] E.P. Murray, T. Tsai, S.A. Barnett, Nature 400 (1999) 649.
[17] C.M. Finnerty, N.J. Coe, R.H. Cunningham, R.M. Ormerod, Catal. Today 46 (1998) 137.
[18] F. Besenbacher, I. Chorkendorff, B.S. Clausen, B. Hammer, A.M. Molenbroek, J.K. Norskov, I. Stensgaard, Science 279 (1998) 1913.
[19] J.R. Rostrup-Nielsen, I. Alstrup, Catal. Today 53 (1999) 311–316.
[20] S. Bebelis, A. Zeritis, C. Tiropani, S.G. Neophytides, Ind. Eng. Chem. Res. 12 (2000) 4920–4927.
[21] Z.L. Zhang, X.E. Verykios, Catal. Today 21 (1994) 589.
[22] M.L. Goula, A.A. Lemonidou, A.M. Efstathiou, J. Catal. 161 (1996) 626.
[23] J.S. Tsang, S.E. Park, H. Chon, Appl. Catal. A 145 (1996) 111.
[24] T. Borowiecki, A. Golebiowski, Catal. Lett. 25 (1994) 309.
[25] T. Borowiecki, G. Giecko, M. Panczyk, Appl. Catal. A 230 (2002) 85.
[26] N.C. Triantafyllopoulos, S.G. Neophytides, J. Catal. 217 (2003) 324.
[27] A.L. Sauvet, J. Fouletier, Electrochim. Acta 47 (2001) 987.
[28] T. Caillot, P. Gelin, J. Dailly, G. Gauthier, C. Cayron, J. Laurencin, Catal. Today 128 (2007) 264–268.
[29] S. Bebelis, S. Neophytides, N. Kotsionopoulos, N. Triantafyllopoulos, M.T. Colomer, J. Jurado, Solid State Ionics 177 (2006) 2087–2091.
[30] S.D. Park, J.M. Vohs, R.J. Gorte, Nature 404 (2000) 265.
[31] R.J. Gorte, H. Kim, J.M. Vohs, J. Power Sources 106 (2002) 10.
[32] S. Tao, John T.S. Irvine, J. Electrochem. Soc. 151 (2) (2004) A252.
[33] J. Liu, B.D. Madsen, Z.Q. Ji, S.A. Barnett, Electrochem. Solid State Lett. 5 (2002) A122.
[34] J. Sfeir, P.A. Buffat, P. Möckli, N. Xanthopoulos, R. Vasquez, H.J. Mathieu, J. Van Herle, K.R. Thampi, J. Catal. 202 (2001) 229.
[35] J.C. Ruiz-Morales, J. Canales-Vazquez, B. Ballesteros-Perez, J. Pena-Martinez, D. Marrero-Lopez, J.T.S. Irvine, P. Nunez, J. Eur. Ceram. Soc. 27 (2007) 4223–4227.
[36] J.R. Rostrup-Nielsen, T.S. Christensen, I. Dybkjaer, Recent Adv. Basic Appl. Asp. Ind. Catal. 113 (1998) 81.
[37] J.J. Strohm, J. Zheng, C.S. Song, J. Catal. 238 (2006) 309.
[38] N.T. Andersen, F. Topsoe, I. Alstrup, J. Rostrup-Nielsen, J. Catal. 85 (1984) 31.
[39] F. Abild-Pedersen, O. Lytken, J. Engbeak, G. Nielsen, I. Chorkendorff, Surf. Sci. 590 (2–3) (2005) 127–137.
[40] R.J. Gorte, J.M. Vohs, J. Catal. 216 (2003) 477.
[41] H. Kim, C. Lu, W.L. Worell, J.M. Vohs, R.J. Gorte, J. Electrochem. Soc. A 149 (2002) 247.
[42] A. Atkinson, S. Barnett, R.J. Gorte, J.T.S. Irvine, A.J. McEvoy, M. Mogensen, S.C. Singhal, J. Vohs, Nat. Mater. 3 (2004) 17.
[43] E. Nikolla, J. Schwank, S. Linic, J. Catal. 250 (2007) 85–93.
[44] J.R. Hansen, P.H. Larsen, J. Electrochem. Soc. 148 (2001) A74.
[45] P. Holtappels, J.T.S. Irvine, M. Mogensen, J. Electrochem. Soc. 148 (2001) A923.
[46] B.A. Boukamp, F. Tietz, Solid State Ionics 135 (2000) 433.
[47] J. Canales-Vázquez, S.W. Tao, J.T.S. Irvine, Solid State Ionics 159 (2003) 159.
[48] O.A. Marina, L.R. Pederson, in: J. Huijsmans (Ed.), Proceedings of the Fifth European Solid Oxide Fuel Cell Forum, European SOFC Forum, Switzerland, 2002, p. 481.
[49] N.C. Triantafyllopoulos, S.G. Neophytides, J. Catal. 239 (2006) 187–199.
[50] S. Zafeiratos, S. Kenou, Surf. Sci. 532 (2003) 402–408.
[51] Ya-Huei Chin, David L. King, Hyun-Seog Roh, Yong Wang, Steven M. Heald, J. Catal. 244 (2006) 153–162.
[52] J. Xu, G.F. Froment, AIChE J. 35 (1989) 88.
[53] S. Zafeiratos, Ph.D. thesis, University of Patras, Greece, 2000.
[54] P.M. Holmblad, J. Wambach, I. Chorkendorf, Molecular beam study of dissociative sticking of methane on Ni(100), J. Chem. Phys. 102 (20) (1995) 8255.
[55] J.H. Sinfelt, J. Catal. 29 (1973) 308.
[56] J.H. Sinfelt, Rev. Mod. Phys. 51 (1979) 569.
[57] H.S. Bengaard, J.K. Nørskov, J. Sehested, B.S. Clausen, L.P. Nielsen, A.M. Molenbroek, J.R. Rostrup-Nielsen, J. Catal. 209 (2002) 365.
[58] J.H. Jun, T.H. Lim, S.-W. Nam, S.-A. Hong, K.J. Yoon, Appl. Catal. A 312 (2006) 27–34.
[59] C.G. Vayenas, S. Bebelis, I.V. Yentekakis, H. Lintz, Catal. Today 11 (3) (1992) 303–442.
[60] T.P. Beebe Jr., D.W. Goodman, B.D. Kay, J.T. Yates, J. Chem. Phys. 87 (4) (1987) 2305.
[61] M.B. Lee, Q.Y. Yang, S.T. Ceyer, J. Chem. Phys. 87 (5) (1987) 2724.
[62] V.I. Avdeev, G.M. Zhidomirov, Kinet. Catal. 35 (2) (1994) 225–231.
[63] P. Kratzer, B. Hammer, J.K. Norskov, J. Chem. Phys. 105 (13) (1996) 5595.
[64] D.J. Klinke II, W. Steffen, L.J. Broadbelt, J. Catal. 178 (1998) 540.
[65] G.G. Tibbetts, J. Cryst. Growth 66 (1984) 632.